HOSTED BY
ELSEVIER
CrossMark
Available online at www.sciencedirect.com
ScienceDirect
Defence Technology 11 (2015) 18−34
www.elsevier.com/locate/dt

Modeling mechanical behaviors of composites with various ratios of matrix−inclusion properties using movable cellular automaton method

A.Yu. SMOLIN [a,b,*], E.V. SHILKO [a,b], S.V. ASTAFUROV [a,b], I.S. KONOVALENKO [a], S.P. BUYAKOVA [a,b,c], S.G. PSAKHIE [a,c,d]

[a] *Institute of Strength Physics and Materials Science SB RAS, Tomsk 634021, Russia*
[b] *Tomsk State University, Tomsk 634050, Russia*
[c] *Institute of High Technology Physics, Tomsk Polytechnic University, Tomsk 634050, Russia*
[d] *Skolkovo Institute of Science and Technology, Skolkovo 143025, Russia*

Received 7 June 2014; revised 14 August 2014; accepted 25 August 2014
Available online 4 December 2014

Abstract

Two classes of composite materials are considered: classical metal−ceramic composites with reinforcing hard inclusions as well as hard ceramics matrix with soft gel inclusions. Movable cellular automaton method is used for modeling the mechanical behaviors of such different heterogeneous materials. The method is based on particle approach and may be considered as a kind of discrete element method. The main feature of the method is the use of many-body forces of inter-element interaction within the formalism of simply deformable element approximation. It was shown that the strength of reinforcing particles and the width of particle-binder interphase boundaries had determining influence on the service characteristics of metal−ceramic composite. In particular, the increasing of strength of carbide inclusions may lead to significant increase in the strength and ultimate strain of composite material. On the example of porous zirconia ceramics it was shown that the change in the mechanical properties of pore surface leads to the corresponding change in effective elastic modulus and strength limit of the ceramic sample. The less is the pore size, the more is this effect. The increase in the elastic properties of pore surface of ceramics may reduce its fracture energy.

Keywords: Composites; Metal ceramics; Zirconia ceramics; Gel; Modeling; Movable cellular automata; Many-body interaction

1. Introduction

Composites are widely used in industry and nature. Usually the composites consist of matrix, which constitutes the main part of the material, and a large number of small sized inclusions. Inclusions, as a rule, have higher physical and mechanical properties and are designed to improve the useful properties of composites. Typical examples are dispersion-reinforced materials and, in particular, metal−ceramic composites [1]. The availability of hard inclusions allows producing the ultra-hard materials for cutting tools, and the antifriction and protecting materials for aircraft building [2], etc. In case of porous materials, the void "inclusions" provide high heat-insulating properties and low specific density [3−5].

Composites consisting of hard matrices with soft inclusions are not practically used in industry. As an exception, we can refer to metal−ceramics for self-lubricated bearings, which are produced by sintering of mixture of iron and carbon powders followed by oil saturation. Much more such materials exist in nature, first of all as fluid-saturated geological media and bone tissues of animals and man.

* Corresponding author. Institute of Strength Physics and Materials Science SB RAS, Tomsk 634021, Russia.
E-mail address: asmolin@ispms.tsc.ru (A.Yu. SMOLIN).
Peer review under responsibility of China Ordnance Society.

http://dx.doi.org/10.1016/j.dt.2014.08.005

It has to be noted that the properties of a composite are often determined by the properties of the components and the fraction of inclusions. They also depend on the size and shape of inclusions as well as the properties of matrix–inclusion interface in a complicated way [6–8]. That is why the problem of composite modeling is very difficult and complex.

An important trend in mechanics of composite is to develop and apply the numerical methods to study the dynamics and peculiarities of mechanical behavior of heterogeneous materials and structures under complex loading conditions. The advantages of numerical modeling in comparison with analytical solutions are associated with the ability to consider complex geometry of the system, to take into account heterogeneous structure of the material as well as to study in details the dynamics of fracture and the related processes of redistribution and dissipation of elastic energy in the surroundings of the crack. At the same time, these advantages make strong demands for the formalism of applied numerical methods.

The most of research on computational mechanics are performed using finite element method. This method belongs to continuum concept in mechanics, i.e., it assumes that the state controlling variables distribute in space continuously. At the same time for modeling the severe distortion and failure of a material, converting finite elements into particles is more effective and promising [9]. In Ref. [10], so-called meshless (or mesh free) method were used for this purpose (namely smoothed particle hydrodynamics and generalized particle algorithms). Strictly speaking, meshless methods are not pure particle ones. They just use the scattered nodes associated with the centers of finite volumes to discretize the continuum mechanics equations in space, i.e., they are really based on continuum approach. Concerning the problem of modeling heterogeneous media, it should be noted that at least 3–5 meshless particles are required to represent a matrix–inclusion interface. A true particle method can describe this interface using just one particle. The principal difference of particle methods from computational methods in continuum mechanics is to replace the continuous representation of a material with an ensemble of interacting particles (at micro-, meso- or macroscopic scale) or point masses (at the atomic scale within the framework of molecular dynamics or Monte-Carlo method). This in turn determines the difference in governing equations as well. In particular, the conventional partial differential equations of continuum mechanics are replaced by Newton–Euler equations governing the motion of discrete ensemble. Constitutive laws for the considered material in tensor form, which conventionally describes the relationship between local stress and strain or their time derivatives, therewith are replaced by the potentials/forces of inter-particle interaction. One of the most important consequences of these features of particle-based methods is an inherent capability of the discrete objects (particles) to change their surroundings (interacting neighbors). This feature makes "discrete" methods extremely attractive for direct modeling of complicated fracture-related processes including multiple fracture accompanied by formation and mixing of large number of fragments [11–17].

The key points determining the behavior of an ensemble of simple deformable discrete elements are the structural form of the expressions for central and tangential interaction between elements and the relationship between these expressions and constitutive law of the modeled material. A conventional approach is based on the use of pair-wise elastic interaction forces which can be treated as springs between elements. Corresponding value of the spring stiffness is derived on the assumption that strain energy stored in a unit cell of deformed element ensemble is equal to the associated strain energy of the equivalently deformed continuum [18,19]. An approximation of pair-wise interaction has a number of important limitations, among which are the following: i) maximum value of Poisson's ratio of element ensemble depending on packing of elements; ii) packing-related artificial anisotropy of mechanical response of the ensemble; iii) fundamental problems in correct simulation of irreversible strain accumulation in ductile materials.

Our research shows that many of these problems can be solved by using many-particle interaction [20–22]. Note that the construction of such relations becomes possible due to using a hybrid computational technique to combine the mathematical formalisms of discrete elements and cellular automata [23]. Many-body formulation of inter-element forces is adopted from the Wiener–Rosenblueth model of cellular automaton interaction [23,24]. This hybrid technique is referred to as movable cellular automaton method (MCA) [21,22,25,27]. The proposed generalized expression for inter-element forces is the ability to establish the relationship between vector parameters of the interaction and tensor parameters of the material constitutive law. It makes possible to implement different models and criteria of elasticity, plasticity and fracture within the mathematical formalism of MCA.

This paper is devoted to the computational study of composite materials consisting of matrix and equiaxial inclusions using MCA method. The main peculiarity of the considered composite is the ratio of mechanical properties of the matrix and inclusions that varies in a wide range. First, we study the classical dispersion-reinforced material based on the example of metal ceramics. Then the porous ceramics with soft gel inclusions are considered. In the last case, the inclusion rigidity is much less than the matrix one. The main attention of the study is paid on the influence of properties and width of inter-phase boundaries on the effective mechanical properties of the composites.

2. Method of movable cellular automata

Within the frame of MCA, it is assumed that any material is composed by a certain amount of finite size elementary objects (automata) which interact among each other and can rotate and move from one location to another, thereby simulating a real deformation process. The automaton motion is governed by the Newton–Euler equations

$$\begin{cases} m_i \dfrac{\mathrm{d}^2 \vec{R}_i}{\mathrm{d}t^2} = \sum\limits_{j=1}^{N_i} \vec{F}_{ij}^{\,\mathrm{pair}} + \vec{F}_i^{\,\Omega} \\ \hat{J}_i \dfrac{\mathrm{d}^2 \vec{\theta}_i}{\mathrm{d}t^2} = \sum\limits_{j=1}^{N_i} \vec{M}_{ij}, \end{cases} \tag{1}$$

where $\vec{R}_i$, $\vec{\theta}_i$, m_i and $\hat{J}_i$ are the location vector, rotation vector, mass and moment of inertia of ith automaton, respectively; $\vec{F}_{ij}^{\,\mathrm{pair}}$ is the interaction force of the pair of ith and jth automata; and $\vec{F}_i^{\,\Omega}$ is the volume-dependent force acting on ith automaton and depending on the interaction of its neighbors with the remaining automata. In the latter equation, $\vec{M}_{ij} = q_{ij}(\vec{n}_{ij} \times \vec{F}_{ij}^{\,\mathrm{pair}}) + \vec{K}_{ij}$, where q_{ij} is the distance from the center of ith automaton to the point of its interaction ("contact") with jth automaton, $\vec{n}_{ij} = (\vec{R}_j - \vec{R}_i)/r_{ij}$ is the unit vector directed from the center of ith automaton to the jth one and r_{ij} is the distance between automata centers (Fig. 1), $\vec{K}_{ij}$ is the torque caused by relative rotation of automata in the pair (see below).

Note that the automata of the pair may represent the parts of different bodies or of one consolidated body. Therefore its interaction is not always really contact one. That is why we put the word "contact" in quotation marks. More of that, as it shown in Fig. 1, the size of the automaton is characterized by one parameter d_i, but it does not mean that the shape of the automaton is spherical. Real shape of the automaton is determined by area of its "contacts" with neighbors. For example, if we use initial FCC packing, then the automata are shaped like a rhombic dodecahedron, but if we use cubic packing, then the automata are cube-shaped.

For locally isotropic media, the volume-dependent component can be expressed in terms of the pressure P_j in the volume of the neighboring automaton j as follows [21,22].

$$\vec{F}_i^{\,\Omega} = -A \sum_{j=1}^{N_i} P_j S_{ij} \vec{n}_{ij}$$

where S_{ij} is the area of interaction surface of automata i and j; and A is a material parameter.

The total force acting on automaton i can be represented as a sum of explicitly defined normal component $\vec{F}_{ij}^{\,n}$ and tangential (shear) component $\vec{F}_{ij}^{\,\tau}$

$$\begin{aligned} \vec{F}_i &= \sum_{j=1}^{N_i} \left(\vec{F}_{ij}^{\,\mathrm{pair}} - AP_i S_{ij} \vec{n}_{ij} \right) \\ &= \sum_{j=1}^{N_i} \left[\left(F_{ij}^{\mathrm{pair},n}(h_{ij}) - AP_j S_{ij} \right) \vec{n}_{ij} + F_{ij}^{\mathrm{pair},\tau} \left(\vec{l}_{ij}^{\,\mathrm{shear}} \right) \vec{t}_{ij} \right] \\ &= \sum_{j=1}^{N_i} \left(\vec{F}_{ij}^{\,n} + \vec{F}_{ij}^{\,\tau} \right) \end{aligned} \tag{2}$$

where $F_{ij}^{\mathrm{pair},n}$ and $F_{ij}^{\mathrm{pair},\tau}$ are the normal and tangential pair interaction forces depending respectively on the automata overlap h_{ij} (Fig. 1(a)) and their relative tangential displacement $\vec{l}_{ij}^{\,\mathrm{shear}}$ (Fig. 1(b)) calculated with taking into account the rotation of both automata [26,27]. Note that, although the last expression of Eq. (2) formally corresponds to the form of element interaction in conventional discrete element models [28–32], it differs fundamentally from them in many-particle central interaction of the automata.

Using homogenization procedure for stress tensor in a particle described in Refs. [27,32], the expression for the components of the average stress tensor in automaton i takes the form

$$\overline{\sigma}_{\alpha\beta}^{i} = \frac{1}{V_i} \sum_{j=1}^{N_i} q_{ij} n_{ij,\alpha} F_{ij,\beta} \tag{3}$$

where α and β denote the axes X, Y, Z of the laboratory coordinate system; V_i is the current volume of automaton i; $n_{ij,\alpha}$ is the α-component of unit vector $\vec{n}_{ij}$; and $F_{ij,\beta}$ is β-component of the total force acting at the point of "contact" between automata i and j.

The mean stress $\overline{\sigma}_{\mathrm{mean}}^{i}$ in the automaton volume at the pressure P_i can be determined from the calculated stress tensor components

$$P_i = -\overline{\sigma}_{\mathrm{mean}}^{i} = -\frac{\overline{\sigma}_{xx}^{i} + \overline{\sigma}_{yy}^{i} + \overline{\sigma}_{zz}^{i}}{3} \tag{4}$$

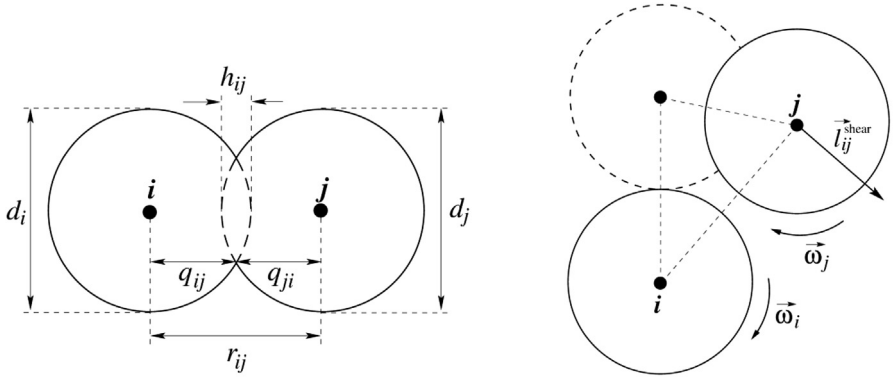

(a) Parameters of central interaction (b) Parameters of tangential interaction

Fig. 1. Schematic diagram of determining of the spatial parameters of a pair of the movable cellular automata i and j.

Tensor components allow us to calculate the other tensor invariants in the automaton volume, in particular stress intensity

$$\overline{\sigma}^i_{\text{int}} = \frac{1}{\sqrt{2}}\sqrt{\left(\overline{\sigma}^i_{xx} - \overline{\sigma}^i_{yy}\right)^2 + \left(\overline{\sigma}^i_{yy} - \overline{\sigma}^i_{zz}\right)^2 + \left(\overline{\sigma}^i_{zz} - \overline{\sigma}^i_{xx}\right)^2 + 6\left[\left(\overline{\sigma}^i_{xy}\right)^2 + \left(\overline{\sigma}^i_{yz}\right)^2 + \left(\overline{\sigma}^i_{xz}\right)^2\right]} \tag{5}$$

From Eqs. (1)–(3) it follows that the specific form of the expressions for $F_{ij}^{\text{pair},n}$ and $F_{ij}^{\text{pair},\tau}$ determines the rheological behavior of a model medium.

For further convenience, the interaction parameters of movable cellular automata are considered in relative (specific) units. Thus, the central and tangential interactions of the automata i and j are characterized by the corresponding stresses η_{ij} and $\overrightarrow{\tau}_{ij}$

$$\begin{cases} F^n_{ij} = \eta_{ij} S_{ij} \\ \overrightarrow{F}^{\tau}_{ij} = \overrightarrow{\tau}_{ij} S_{ij} \end{cases} \tag{6}$$

Note that, in the most of papers devoted to the description and use of MCA, the equations and formulas of the method are written for two-dimensional case. This study uses three-dimensional version of the MCA method. That is why herein shear stress $\overrightarrow{\tau}_{ij}$ is a vector in the plane which is normal to $\overrightarrow{n}_{ij}$.

To characterize the deformation of automaton i under the normal interaction of automata i and j, we can use the following dimensionless parameter (normal strain)

$$\xi_{ij} = \frac{q_{ij} - d_i/2}{d_i/2} \tag{7}$$

In general case, each automaton of a pair represents different material, and the overlap of the pair is distributed between ith and jth automata

$$\Delta h_{ij} = \Delta q_{ij} + \Delta q_{ji} = \Delta\xi_{ij} d_i/2 + \Delta\xi_{ji} d_j/2 \tag{8}$$

where symbol Δ denotes the increment of a parameter per time step Δt of numerical integration of the motion equation (1). The distribution rule of strain in the pair is intimately associated with the expression for computing the interaction forces of the automata. This expression for central interaction is similar to Hooke's relations for diagonal stress tensor components

$$\Delta\eta_{ij} = 2G\left(\Delta\xi_{ij}\right) + \left(1 - 2G/K\right)P_i \tag{9}$$

where K is the bulk modulus; G is the shear modulus of the material of ith automaton; and P_i is the pressure of automaton i, which may be computed using Eqs. (3) and (4) at previous time step or by predictor-corrector scheme.

To determine a parameter characterizing shear deformation in pair of automata i–j, we start with kinematics formula for free motion of the pair as a rigid body

$$\overrightarrow{v}_j - \overrightarrow{v}_i = \overrightarrow{\omega}_{ij} \times \overrightarrow{r}_{ij} \tag{10}$$

where $\overrightarrow{r}_{ij} = (\overrightarrow{R}_j - \overrightarrow{R}_i)$, $\overrightarrow{v}_i$ is the translation velocity of the ith automaton centroid; and $\overrightarrow{\omega}_{ij}$ is the rotational velocity of the pair as a whole (rigid body). If we multiply both sides of Eq. (10) on the left by $\overrightarrow{r}_{ij}$ and neglect rotation about axis connecting centers of the automata of the pair (i.e. let $\overrightarrow{\omega}_{ij} \cdot \overrightarrow{r}_{ij} = 0$ because the rotation about the axis of the pair does not produce a shear deformation), then we get the following formula

$$\overrightarrow{\omega}_{ij} = \frac{\overrightarrow{r}_{ij} \times \left(\overrightarrow{v}_j - \overrightarrow{v}_i\right)}{\overrightarrow{r}^2_{ij}} = \frac{\overrightarrow{n}_{ij} \times \left(\overrightarrow{v}_j - \overrightarrow{v}_i\right)}{r_{ij}} \tag{11}$$

Besides such rotation of the pair as a whole (defined by the difference in translational velocities of the automata), each automaton rotates with its own rotational velocity $\overrightarrow{\omega}_i$ (Fig. 2). The difference between these rotational velocities produces a shear deformation. Thus, the increment of shear deformations of automata i and j per time step Δt is defined by the relative tangential displacement at the contact point $\Delta l_{ij}^{\text{shear}}$ divided by the distance between the automata

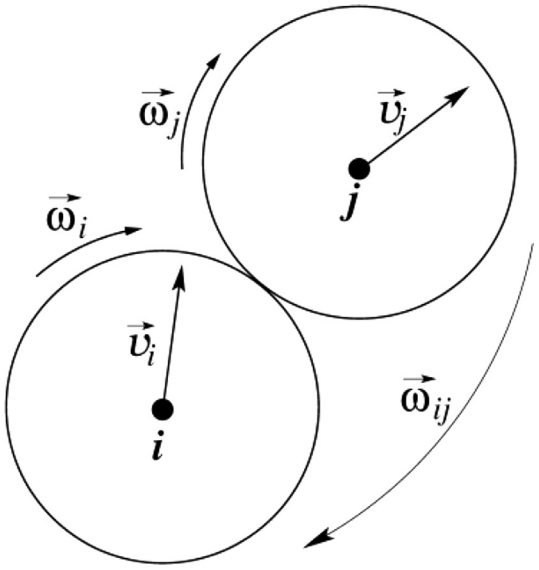

Fig. 2. Translational and rotational velocities of the automata.

$$\Delta\vec{\gamma}_{ij}+\Delta\vec{\gamma}_{ji}=\frac{\Delta\vec{l}_{ij}^{\,\mathrm{shear}}}{r_{ij}}=\frac{\left(q_{ij}\left(\vec{\omega}_{ij}-\vec{\omega}_i\right)\times\vec{n}_{ij}+q_{ji}\left(\vec{\omega}_{ij}-\vec{\omega}_j\right)\times\vec{n}_{ij}\right)\Delta t}{r_{ij}} \tag{12}$$

The expression for tangential interaction of movable cellular automata is similar to Hooke's relations for non-diagonal stress tensor components

$$\Delta\vec{\tau}_{ij}=2G\left(\Delta\vec{\gamma}_{ij}\right) \tag{13}$$

and is pure pairwise.

The difference in automaton rotation leads also to the deformation of relative "bending" and "torsion" (only in 3D) of the pair (Fig. 3). It is obvious that the resistance to relative rotation in the pair cause the torque, which value is proportional to the difference between the automaton rotations

$$\vec{K}_{ij}=-\left(G_i+G_j\right)\left(\vec{\theta}_j-\vec{\theta}_i\right) \tag{14}$$

Eqs. (1)–(4), (6)–(9), (11)–(14) describe the mechanical behavior of a linearly elastic body in the framework of MCA method. Note that Eqs. (8), (9), (12) and (13) are written in increments, i.e., in the hypoelastic form. In Ref. [33] it is shown that this model gives the same results as the numerical solving usual equation of continuum mechanics for isotropic linearly elastic medium by finite-difference method. That makes it possible to couple MCA method with the numerical methods of continuum mechanics. The results in Ref. [26] show that the rotation allows the movable cellular automata correctly to describe the isotropic response of material.

We propose to use the plastic flow theory (namely von Mises model) for the description of elastoplastic behavior within the MCA method. For this purpose Wilkins' algorithm [34] is adapted to the MCA method [27,40]. It is well known that Wilkins' radial return algorithm consists in the solution of elastic problem in the increments and subsequent "drop" of components of deviator stress tensor $D_{\alpha\beta}=\sigma_{\alpha\beta}-1/3\sigma_{kk}\delta_{\alpha\beta}$ to von Mises yield surface in the case that stress intensity exceeds it (Fig. 4)

$$D'_{\alpha\beta}=D_{\alpha\beta}\bullet M$$

where $M=\sigma_{\mathrm{pl}}/\sigma_{\mathrm{int}}$, σ_{int} is stress intensity; and σ_{pl} is current radius of von Mises yield circle.

This algorithm, as applied to the automaton i, can be written in the following notation

$$\begin{cases}\left(\overline{\sigma}^i_{\alpha\alpha}\right)'=\left(\overline{\sigma}^i_{\alpha\alpha}-\overline{\sigma}^i_{\mathrm{mean}}\right)M_i+\overline{\sigma}^i_{\mathrm{mean}}\\ \left(\overline{\sigma}^i_{\alpha\beta}\right)'=\overline{\sigma}^i_{\alpha\beta}M_i\end{cases} \tag{15}$$

where $\alpha,\beta=X,Y,Z$ and $\alpha\neq\beta$, $\left(\overline{\sigma}^i_{\alpha\alpha}\right)'$ and $\left(\overline{\sigma}^i_{\alpha\beta}\right)'$ are the returned (corrected) average stress tensor components; $\overline{\sigma}^i_{\alpha\alpha}$ and $\overline{\sigma}^i_{\alpha\beta}$ are the components of stress tensor, which result from the solution of elastic problem at the current time step; $M_i=\sigma^i_{\mathrm{pl}}/\overline{\sigma}^i_{\mathrm{int}}$ is the current value of the coefficient M for the automaton i; and σ^i_{pl} is the current radius of von Mises yield circle for the automaton i.

By analogy with the elastic problem, the specific normal and tangential interaction forces are corrected with the use of the current value of coefficient M by directly reforming Wilkins' algorithm for average stress (Eq. (15))

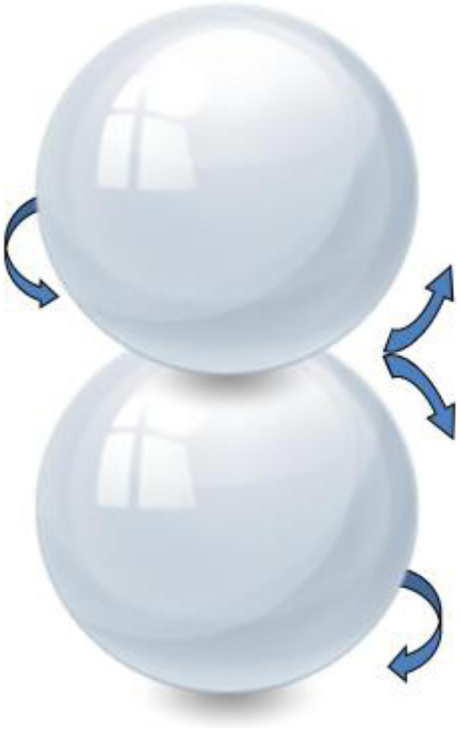

Fig. 3. Deformation due to relative rotation between automata.

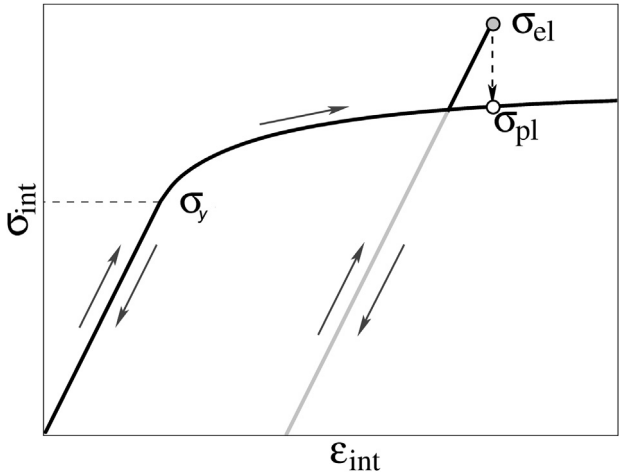

Fig. 4. Schematic of functioning of Wilkins' radial return algorithm.

$$\begin{cases} \eta'_{ij} = (\eta_{ij} - P_i)M_i + P_i \\ \tau'_{ij} = \tau_{ij} M_i \end{cases}$$

where η'_{ij} and τ'_{ij} are the corrected specific forces. It is easy to show that the substitution of these relations for Eqs. (2) and (3) automatically ensures to return the components of average stress tensor in the automaton to the yield circle.

Thus, the rheological properties of the material of the automaton i are determined by defining a unified hardening curve $\overline{\sigma}^i_{\text{int}} = \Phi(\overline{\varepsilon}^i_{\text{int}})$ (here $\overline{\varepsilon}^i_{\text{int}}$ is the average intensity of strain tensor that can be computed, similar to $\overline{\sigma}^i_{\alpha\beta}$ [27,32]); this dependence is also named as automaton response function.

The equations of motion, i.e., Eq. (1), for the system of movable cellular automata are numerically integrated with the use of velocity Verlet algorithm modified by introducing a predictor for estimation of $\overline{\sigma}^i_{\alpha\beta}$ at the current time step [35].

A pair of elements might be considered as a virtual bistable automaton having two stable states (bound and unbound), which permits simulation of fracture and coupling of fragments (or crack healing) by MCA. These capabilities are taken into account by means of corresponding change of the state of the pair of automata (Fig. 5(a)). A fracture criterion depends on the physical mechanisms of material deformation. An important advantage of the formalism described above is that it makes possible direct application of conventional fracture criteria (Huber–Mises–Hencky, Drucker–Prager, Mohr–Coulomb, Podgorski, etc.), which are written in tensor form.

To use a conventional fracture criterion for breaking inter-automaton bond, the local stress tensor at the area of interaction ("contact" area) of the considered pair i–j (hereinafter we denote this tensor as $\sigma^{ij}_{\alpha'\beta'}$) has to be determined. For simplicity, the definition of this tensor is shown below for 2D case (an extension to general 3D case is trivial).

In the local coordinate system $X'Y'$ of the pair (Fig. 5(b)), the components $\sigma^{ij}_{y'y'}$ and $\sigma^{ij}_{x'y'}$ for the pair i–j are numerically equal to the specific forces of central (σ_{ij}) and tangential (τ_{ij}) interaction of the automata (these forces are applied to the "contact" area S_{ij}). The other components ($\sigma^{ij}_{x'x'}$ and $\sigma^{ij}_{z'z'}$) of local stress tensor in the local coordinate system $X'Y'$ are defined on the basis of linear interpolation of the corresponding values ($\overline{\sigma}^i_{x'x'}$ and $\overline{\sigma}^j_{x'x'}$, $\overline{\sigma}^i_{z'z'}$ and $\overline{\sigma}^j_{z'z'}$) for the automata i and j to the area of interaction

$$\begin{cases} \sigma^{ij}_{x'x'} = \left(\overline{\sigma}^i_{x'x'} q_{ji} + \overline{\sigma}^j_{x'x'} q_{ij}\right)/r_{ij} \\ \sigma^{ij}_{z'z'} = \left(\overline{\sigma}^i_{z'z'} q_{ji} + \overline{\sigma}^j_{z'z'} q_{ij}\right)/r_{ij} \end{cases} \tag{16}$$

where $\overline{\sigma}^i_{\alpha'\beta'}$ and $\overline{\sigma}^j_{\alpha'\beta'}$ are the components of average stress tensor in the volume of automata i and j in the local coordinate system of the pair.

Thus the defined components $\sigma^{ij}_{\alpha'\beta'}$ can be used for calculating the necessary tensor invariants which then can be used to calculate the current value of the fracture criterion applied. For example, the unbinding condition for the pair i–j based on the fracture criteria of Drucker and Prager is as follows

$$\sigma^{ij}_{\text{eq}} 0.5(a+1) + \sigma^{ij}_{\text{mean}} 1.5(a-1) = \sigma_{\text{c}} \tag{17}$$

where σ_{c} is the corresponding threshold value for the pair (strength of cohesion/adhesion); $a = \sigma_{\text{c}}/\sigma_{\text{t}}$ is the ratio of compressive strength (σ_{c}) to tensile strength (σ_{t}) of the pair bond; and σ^{ij}_{eq} and $\sigma^{ij}_{\text{mean}}$ are the corresponding invariants of the stress tensor $\sigma^{ij}_{\alpha'\beta'}$.

When the explicit scheme of integration of motion equations is used, the value of time step Δt is limited from above by a quantity associated with the time of sound propagation through the bulk of element. Normally the time step is equal to or less than a quarter of this limit. In such a situation the conventional model of bond breaking during one time step Δt is an idealized condition because it virtually suggests that the spatial separation of atomic layers occurs uniformly over the whole surface of interaction of elements. Herein the following approach is suggested for more accurate description of the crack growth dynamics. It is assumed that the breaking of a bond (linked → unlinked transition of the pair state) is a process distributed in time and space. To express it numerically, we propose to use the dimensionless factor k^{ij}_{link} ($0 \le k^{ij}_{\text{link}} \le 1$) which has the meaning of the portion of linked part of the contact area S_{ij}. In this case, the linked part of the contact area in the pair i-j is expressed as $S^{ij}_{\text{link}} = S_{ij} k^{ij}_{\text{link}}$. Thus, the dynamics of bond breaking is determined by the dependence $k^{ij}_{\text{link}}(t)$, where k^{ij}_{link} decreases from the initial value 1 (totally linked pair) to the final value 0 (totally unlinked pair). Depending on the automaton size and features of the internal structure of the material the stable or unstable crack growth models can be applied to describe the pair bond breaking.

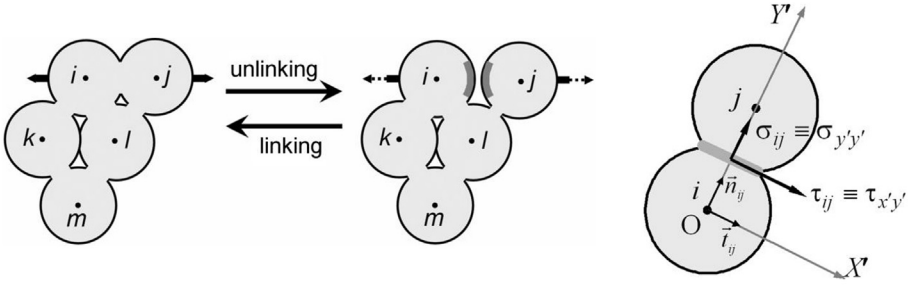

(a) Switching between bound (at the left) and unbound (at the right) states

(b) Definition of instantaneous coordinate system $X'Y'$

Fig. 5. Schematic diagram of the interacting pair of automata i and j.

In the first model (stable crack growth), the process of fracture develops in accordance with the predefined dependence

$$\mathrm{d}k_{\mathrm{link}}^{ij}/\mathrm{d}\varepsilon_{\mathrm{int}}^{ij} = f\left(\varepsilon_{\mathrm{eq}}^{ij}, k_{\mathrm{link}}^{ij}, \dot{\varepsilon}_{\mathrm{eq}}^{ij}, \ldots\right) < 0$$

where $\varepsilon_{\mathrm{eq}}^{ij}$ is the pair equivalent strain which can be calculated, for example, using the components of the strain tensor $\varepsilon_{\alpha\beta}^{ij}$ defined by analogy with $\sigma_{\alpha\beta}^{ij}$. In the simplest case, this dependence can be considered as a constant.

In the second model (unstable crack growth), it is assumed that, if the fracture criterion threshold is exceeded, then a crack begins to grow spontaneously according to the somehow specified law

$$\mathrm{d}k_{\mathrm{link}}^{ij}/\mathrm{d}t = f\left(t, k_{\mathrm{link}}^{ij}\ldots\right) < 0$$

where t is time. In the simplest case, this dependence can be considered as a constant, which means that the crack advances through the pair interaction area at the constant velocity V_{crack}. The value of V_{crack} is a predefined (model) parameter, which reflects the rheology of the interface material between the interacting elements. In particular, for brittle materials, V_{crack} could be close to Raleigh wave speed, while for ductile materials, its value should obviously be significantly smaller.

The distinctive features of interaction of "unlinked" (i.e., contacting) automata i and j, among others, are (i) lack of resistance to tension (a pair is considered as interacting one if $\sigma_{ij} \leq 0$ only); and (ii) limited magnitude of the force of tangential interaction. Maximum value of the tangential force (τ_{ij}) allowed between "unlinked" automata is determined by the model of friction applied (for example, Amonton's law, model of Dieterich and so on).

3. Study of particle-reinforced metal–ceramic composites

Metal–ceramic composites (MCC) are the advanced representatives of dispersion-reinforced materials, which have the enhanced values of mechanical and service characteristics, such as strength, stiffness-to-weight ratio, crack growth resistance, wear resistance, fracture energy, ratio of thermal conductivity to thermal expansion coefficient, thermal stability and so on. This makes them very attractive for widespread use in various industries, such as materials for extreme operating conditions [2,36]. At the present time, the working parts of machines and mechanisms operating under the conditions of shock loading, abrasion, high temperature and corrosive environment are made mostly of metal–ceramic composites on the basis of very hard and refractory compounds (carbides, nitrides, carbonitrides) with metallic binder (nickel and iron alloys) [1,2,37]. These materials are fabricated from the powder mixtures of the compounds by powder metallurgy methods [2,38]. The mechanical and physical properties of the sintered metal–ceramic composite are determined, in addition to phase composition, by a number of structural factors (volume fraction, dispersion, geometry and faultiness of reinforcing particles, structural-phase state of metallic binder, etc. [2,39,40]).

Numerical simulation is of great importance for studying the mechanical properties of composite materials and their dependence on geometric and mechanical characteristics of inclusion-matrix interfaces. In this paper, MCA method is applied to study the influence of reinforced ceramic inclusions and geometric (width) properties of inclusion-binder interphase boundaries on the peculiarities of mechanical response of metal–ceramic composite under dynamic loading. TiC-particle-reinforced Ni–Cr matrix composite (50 vol.% of TiC inclusions with average size of 3 μm) is chosen as a model system classified as metal–ceramic composite material in which the inclusions are much stiffer than the binder.

Note that, for correct simulation of mechanical response of such complex heterogeneous materials, it is necessary to take into account main features of their internal structure. For this purpose, a two-dimensional structural and rheological model of MCC in the framework of MCA method was proposed in the paper. In this model, each of the composite constituents is simulated by an ensemble of movable cellular automata with appropriate rheological parameters (thus the cellular automaton simulates a domain/fragment of an inclusion, or a binder, or an interface zone). As an example of MCA-based structural model, Fig. 6(a) shows the structure of an idealized metal–ceramic composite with TiC particles having an equiaxed shape and the average size D_{TiC} of 3 μm. The components of the metal–ceramic composites have very different rheological characteristics (in case of considered composite these are elastic-brittle high-strength TiC inclusions and elastic–plastic NiCr binder). For correct modeling of deformation and fracture of such complex systems, the mathematical formalism of constructing many-particle interaction forces for cellular automata (discrete elements) with different rheological characteristics was developed [27,33,41].

In the following calculations, the plane stress approximation is used. The elastic constants and diagram of uniaxial loading of the material are used as the input parameters of the model to characterize the inter-element interaction (the mechanical response function of movable cellular automaton). The response function of automaton modeling NiCr is considered as a stress–strain diagram with linear hardening (Curve 1 in Fig. 6(b)). This diagram is an approximation of the experimental diagram of uniaxial compression of macroscopic samples of the alloy. The mechanical properties of the automata that simulate the high-strength brittle inclusions meet the real properties of TiC particles in the ceramic phase (polycrystalline particles, Curve 2 in Fig. 6(b)). Two-parameter Drucker–Prager fracture criterion in Eq. (17) is used to describe the fractures of metallic binder and carbide particles in the developed model [27,33,41]. Thus, in this work, the strength characteristics of the composite material are determined by the tensile (σ_{t}) and compressive (σ_{c}) strength of its components.

The developed model was used for investigating the influence of the main features of internal structure on the basic characteristics of mechanical behavior of the metal–ceramic composite. For this purpose, a three-point bending test [42,43] of the model samples of MCC was simulated. The structure of

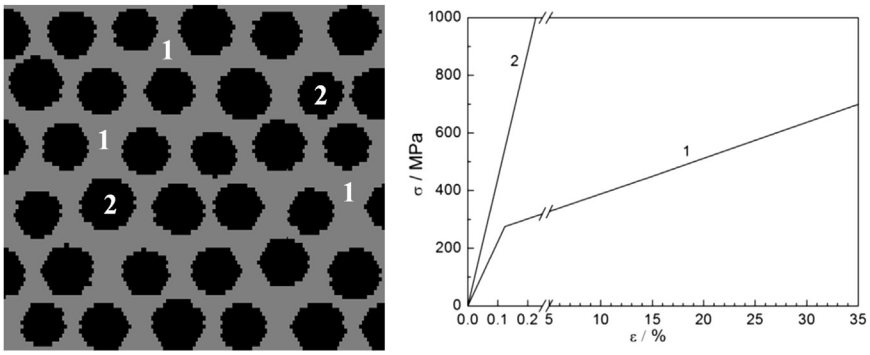

(a) Structural model (b) Properties of components

Fig. 6. The model of metal–ceramic composite and the response functions of movable cellular automata of its components. Main components of the structure are plastic nickel–chromium binder (1) and high-strength brittle titanium carbide inclusions (2).

the model set-up is shown in Fig. 7. Dynamic loading of 20 μm cylindrical mandrel at constant velocity $V_{load} = 0.5$ m/s was applied to the sample of 24 × 130 μm in dimensions. The value of the maximal resistance of the sample to bending and the corresponding displacement of the mandrel, as well as the dynamics and pattern of the sample fracture were analyzed.

It is well known that the strength of reinforcing particles largely determines the integral characteristics of the composite. Cracking of particles, containing significant (large) internal defects and damages, leads to the nucleation of internal cracks at lower applied loads and furthermore accelerates the crack growth. As a consequence, such integrated mechanical characteristics of the composite as strength and deformation ability could substantially reduce. Therefore, the influence of the strength of the TiC particles, which characterizes their initial defect structure or density of damages, on the integral mechanical response of the material was analyzed in the paper. It should be noted that the compressive and tensile strengths of brittle materials can differ by an order of magnitude ($\sigma_c >> \sigma_t$). The physical reason of this difference is that the damages, which initially exist and emerge in the process of loading, function in different ways under the action of compressive and tensile stresses. In conditions of compression (including uniaxial), the surfaces of a damage could occlude. This leads to their relative resistance to compression and shear (because of adhesion and dry friction of the damage surfaces). A spatial diversity of the damage surfaces occurs under the conditions of tension. Since the edges of damages are the stress concentrators, the absence of plastic deformation provides the conditions for the fast growing of damages and

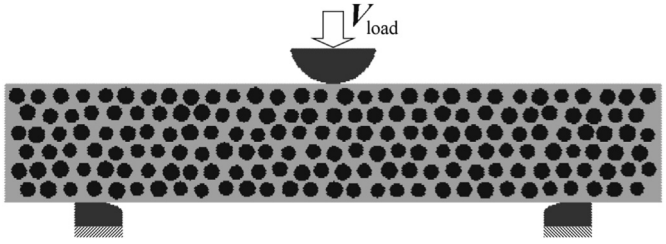

Fig. 7. Scheme of the simulated three-point bending test of the model composite sample.

cracks. Thus, the key strength characteristic, which determines the integral strength of TiC particles in the composite, is its tensile strength (σ_t). In the paper, the value of σ_t varied from 700 MPa that corresponds to the tensile strength of the metallic binder NiCr to 2000 MPa. The choice of this interval is determined by the known fact that the tensile strength of real samples with typical dimensions of 1 ÷ 10 microns are generally 15 ÷ 50 times less than the theoretical strength of material (44 ÷ 88 GPa for TiC in the case of absence of large damages). The value of σ_c for TiC particles in all calculations was equal to 10,000 MPa.

Note that the so-called model of "narrow" particle-binder interfaces [7] is used in the calculation presented below. In this model, it is assumed that the width of the interphase boundary is much smaller than the size of movable cellular automaton. Moreover, the assumption of ideal adhesion of the composite components (TiC inclusions and NiCr binder) was used. This assumes that the strength characteristics of the interface are equal to the corresponding values for the least durable component of the composite material (in this case Ni–Cr alloy). Use of this approach allows to study the influence of the strength characteristics of carbide inclusions on the mechanical response of the composite in the raw.

Fig. 8 shows the dynamic loading of the simulated composite samples with different values of tensile strength of TiC inclusions. The diagram is plotted in terms of normalized stress σ/σ_t^{NiCr} versus bending angle. Here the stress σ is defined as resistance force of composite applied on mandrel divided by the area of the upper surface of the mandrel, $\sigma_t^{NiCr} = 700$ MPa is the tensile strength of NiCr binder. It could be seen from Fig. 8 that the strength and deformation characteristics of the composite (Curves 3 and 4) are decreased at tensile strength of TiC inclusions (σ_t^{TiC}) less than 1100 MPa. In particular, the decrease in σ_t^{TiC} to the value of tensile strength of metallic binder leads to a twofold decrease in ultimate strain.

As could be seen from Fig. 8, the essential change in the mechanical parameters of the composite occurs in a fairly narrow strength interval of TiC inclusions and has a threshold character. Analysis of the fracture dynamics of the model samples shows that this is due to the active involvement of

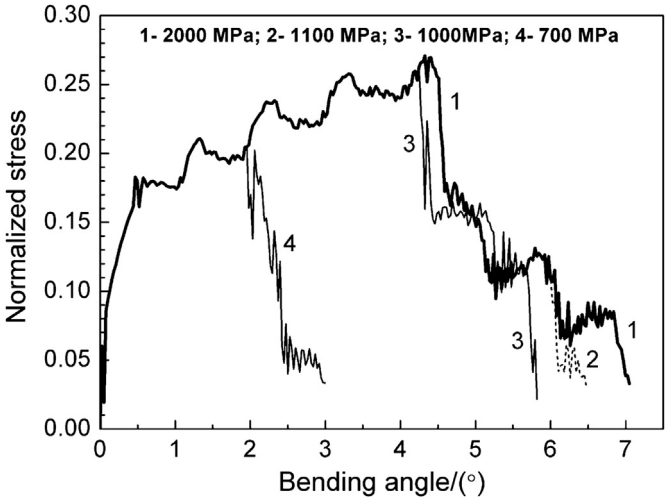

Fig. 8. The loading diagrams (normalized stress σ/σ_t^{NiCr} versus bending angle) for the model samples of metal–ceramic composite with different strength σ_t^{TiC} of TiC inclusions under three-point bending test.

cracking mechanism of low strength ($\sigma_t^{TiC} < 1100$ MPa) TiC particles in the process of composite fracture. Fig. 9 shows the main stages of fracture of the composites with different strength values of TiC inclusions. It could be seen from Fig. 9 that, in the composites with high-strength inclusions, the cracks are nucleated and propagated in the matrix by passing the reinforcing particles along the interphase boundaries ($\sigma_t^{TiC} = 2000$ MPa, top row in Fig. 9). For the composites with particles having a tensile strength approaching to the threshold value, the cracks are generated and propagated in the binder, but they "cut" them ($\sigma_t^{TiC} = 1000$ MPa, middle row in Fig. 9) when they reach to TiC particles. Further decrease in the particle strength leads to a change in fracture mechanism of the composite. As could be seen from Fig. 9 (bottom row), fracture begins at the bottom part of the sample (in the area of maximum tensile stress) by means of nucleation of cracks in ceramic particles. Then, with the increase in the applied strain, these cracks consequently connect with the cracks passing through the binder into a single main crack. This change in the fracture mechanism is accompanied by the significant decrease in integral deformation characteristics of the composite. Thus, the strength of the reinforcing inclusions is one of the most important factors determining a number of service characteristics of metal–ceramic composites, such as strength, critical deformation, fracture toughness, and others.

It should be noted that one of the key elements of the internal structure of the metal–ceramic composites is the interface between the particles of refractory compounds and the metallic binder. The change in the technological peculiarities of metal–ceramic composite fabrication (in particular, applying additional heat treatment of the composite) can vary the geometry (width) of interphase boundaries and, consequently, their mechanical properties [7]. Therefore, the influence of this factor on the mechanical characteristics of MCC was investigated in the paper. The investigation was carried out using a mesoscopic model of "wide" interphase boundary (transition zone). In this model, it is assumed that the width of the interface is comparable to or greater than the size of the movable cellular automaton [7]. Here the particle-binder interface is regarded as an area of variable composition of chemical elements (Ti, Ni, Cr, C) and modeled by several layers of cellular automata. In this area, the volume fractions of TiC and NiCr vary with a distance from the particle surface to the bulk of binder according to a given law. This leads to an appropriate change in the physical and mechanical (including response function and strength parameters σ_c and σ_t) characteristics of these "transition" automata. This model can be efficiently used in numerical simulation of composites in the case of the width of the transition zone higher than the size of the cellular automaton.

The existing experimental data on the structure of particle-binder interfaces show that these areas contain a significant amount of secondary dispersed particles of titanium carbide (with the size of 50 ÷ 100 nm) [1,7,38]. The volume content of this particles decreases with the increase in distance from particle surface to the bulk of binder. In the paper, this factor is considered using so-called multiscale approach. In the framework of this approach, the elements of the internal structure of the composite at the mesoscopic scale (binder, primary particles TiC and wide interphase boundaries) are taken into account explicitly. Taking into account structural elements of lower scales (in particular, the presence of secondary titanium carbide nanoparticles in the interphase boundaries) is carried out by considering the structural models of lower scales (in this case the submicron scale) with explicit prestoring concentrations, sizes and spatial distribution of nanoscale elements. On the base of analysis of simulation results of mechanical tests of submicron-sized samples their integral mechanical (including rheological) properties are determined. In the subsequent, they are used as input data for cellular automata modeling composite response at the mesoscopic scale. Thus, using of the multiscale approach allows to obtain the dependence of mechanical properties of the interphase boundaries on local concentration of the nanoparticles of the carbide phase.

The influence of the width of interphase boundaries on the integral mechanical characteristics of metal–ceramic composite is investigated hereafter. Fig. 10 shows the loading diagrams of the composite samples with different width of particle-binder interfaces. It could be seen from Figs. 10 and 11 that the increase in the width of the interphase boundaries leads to the increase in the strength of the composite, as well as the increase in the value of the ultimate strain (critical value of bending angle in the considered test). As follows from the analysis of dependencies presented in Fig. 11, the main effect of increasing the width of the interphase boundaries up to 1.6 microns is manifested in the increase in the critical strain of the material (up to 2 times).

Analysis of the results of computer simulation show that the increase in strength and value of ultimate strain of the composite material with the increase in width of the interphase boundaries is due to the significant expansion of the region of the stress reducing from the high value in the reinforcing

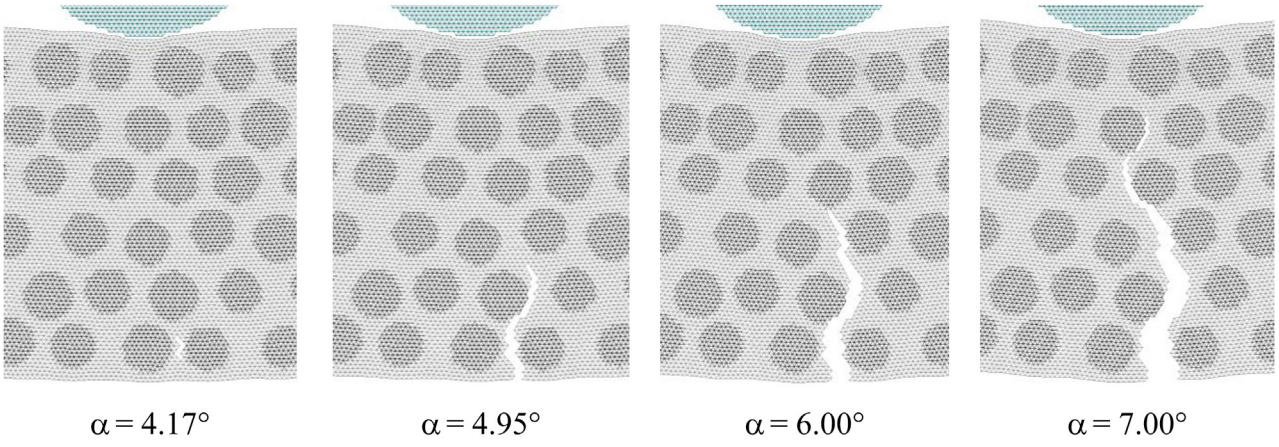

(a) 2000 MPa

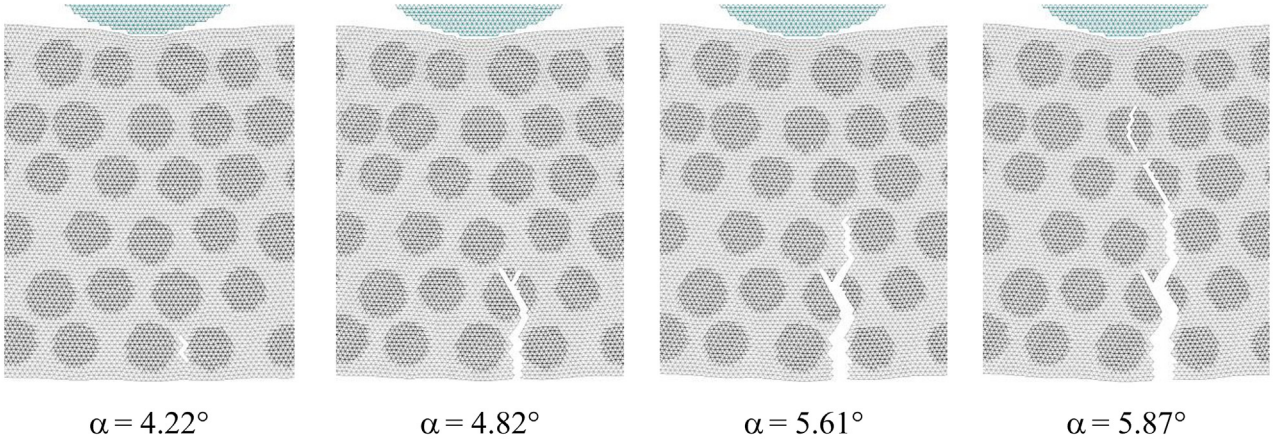

(b) 1100 MPa

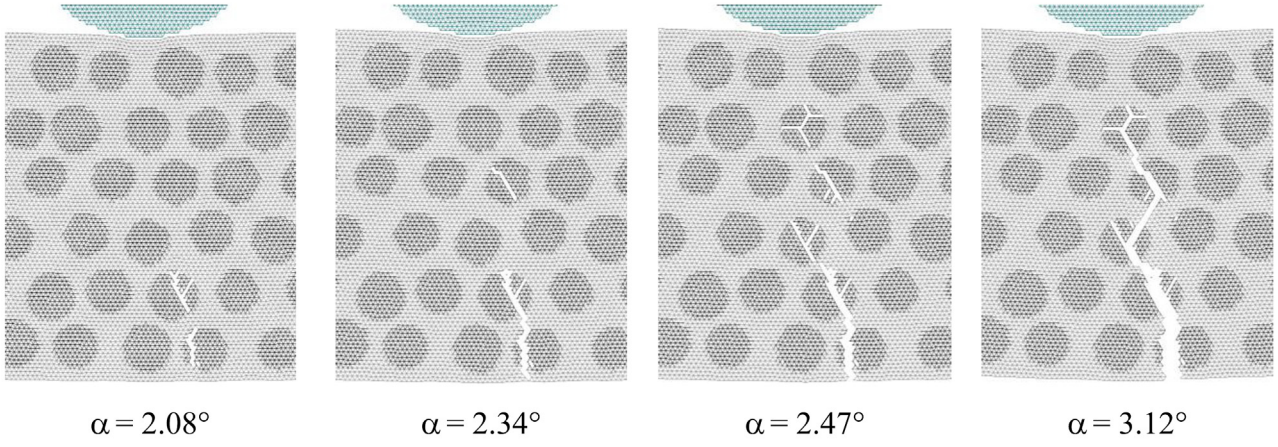

(c) 1100 MPa

Fig. 9. Dynamics of fracture in metal–ceramic composite samples characterized by different strength values of TiC inclusions σ_t^{TiC}. Here α is the bending angle.

particles (which are the stress concentrators in the composite) to the significantly lower value in the plastic binder. Von Mises stress distributions for the samples which are characterized by different widths of interphase boundaries are shown in Fig. 12. It can be seen from Fig. 12 that the formation of wide transition zones around the reinforcing particles, which are characterized by a smooth change of the mechanical characteristics with the distance from the surface of the ceramic inclusion to the bulk of the binder, leads to "smearing" the stress field and, consequently, to reducing the stress gradient at

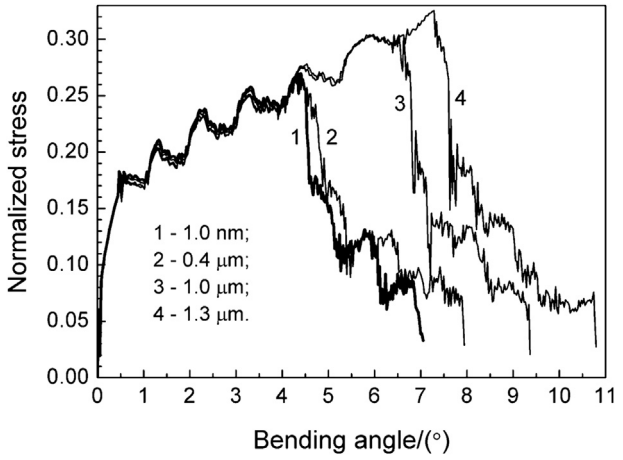

Fig. 10. Loading diagrams for the model samples of metal–ceramic composite with different width of particle-binder interface.

the interface. This means that the formation of wide interphase boundaries among reinforcing particles and metallic binder interfaces in metal–ceramic composites provides a relatively low level of stress in the transition zones. This leads to increasing the deformation ability and strength of the modified surface layers.

It is necessary to note that the results obtained herein by simulation are in good agreement with the existing experimental data. As pointed out in Ref. [40], the constraint imposed on matrix plastic deformation by the ceramic reinforcements induces large tensile hydrostatic stresses in the matrix. This enhances the load carried by the reinforcements and hence the composite flow stress, and also triggers the early development of internal damage in the form of particle fracture, interface decohesion, and/or matrix void growth. New experimental techniques, such as automated serial section and X-ray computed microtomography (XCT), provide detailed information on the relationship between the damage nucleation or growth and specific features of the three-dimensional microstructure [40,42]. The experiments with model materials, presented in Ref. [40], show that the damage of the model

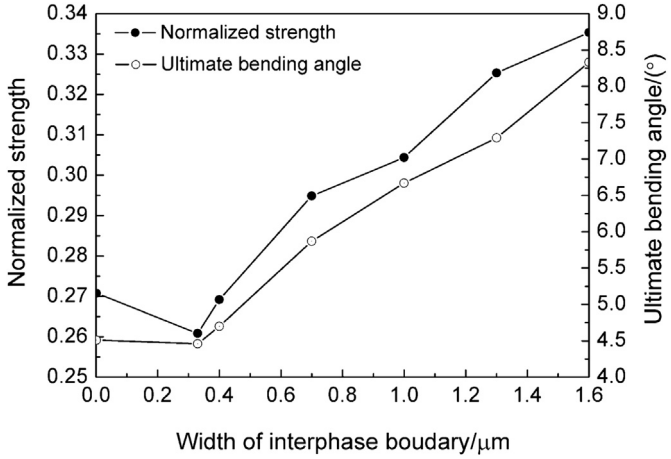

Fig. 11. Dependencies of normalized strength of the model metal–ceramic composite and its ultimate bending angle on width of interphase boundary.

composite material made of a soft matrix is mainly attributed to decohesion along the particle/matrix interface, while for the material with the same structure but with a harder matrix, the damage mechanism changes to particle fracture. In Ref. [42], for a notched glass fiber/epoxy cross-ply laminate subjected to three-point bending, the onset and evolution of the damage in three dimensions were studied by XCT. It was found that the damage began by formation of intra-ply cracks in the 90° plies followed by intra-ply cracking in the 0° plies.

Our simulation results also explain that such a perspective way can improve the mechanical characteristics of metal–ceramic composites if the high-strength multiscale thermally stable structures are formed in their surface layers under the impact of concentrated streams of charged particles. For example, the electron-beam irradiation on the surface layers of metal–ceramic alloy containing 50 vol.% of TiC and 50 vol.% of NiCr leads to a considerable increase in the mechanical and operating characteristics of the material [44,45]. The experimental results [44,45] showed that the increase in the operating characteristics of modified composite is due to a number of factors. Among them are the significant increase in the width of the interphase boundary between the matrix and reinforcing particles and the formation of a significant amount of secondary nanosized particles of TiC among these transition zones. Furthermore, the superfast heating of surface layer leads to the fragmentation and partial dissolution of most damaged carbide inclusions, and to the healing of small defects which are contained in the reinforcing TiC particles. The direct consequence of this is a significant increase in the strength (including tensile strength) of ceramic inclusions and the integral operational properties of the material.

Fig. 13 shows the change of temporal durability at cutting and the micro-hardness of MCC TiC–NiCr after pulsed electron beam irradiation in nitrogen-containing gas discharge plasma. It can be seen from Fig. 13 that the operating characteristics of the composite can be considerably improved by the electron-beam treatment of the surface layers of the material.

4. Study of porous ceramics with gel

The next part of the paper is devoted to modeling the porous ceramics filled with gel, which matrix stiffness and strength are much higher than those of the inclusions. $ZrO_2(Y_2O_3)$ based ceramics was used as a matrix [3,4]. There are three maxima in pore size distribution bar chart for this material: 1 μm; 2 μm (comparable with grain size); 6 μm (cells). Gel-forming composition GALKA, developed for enhancing oil recovery [46], was used as the filler of the composite. In Ref. [47], gel filling was performed through spontaneous soaking of ceramics samples by initial gel-forming liquid composition during 24 h. Soaking occurs due to capillary effect. Then, the soaked sample was baked to form the gel at 80 °C for 1 h; the sample cooled in a kiln. Mechanical testing of the soaked ceramics showed that their mechanical properties depends on the structure of the initial ceramics powder. Corresponding experimental data are shown

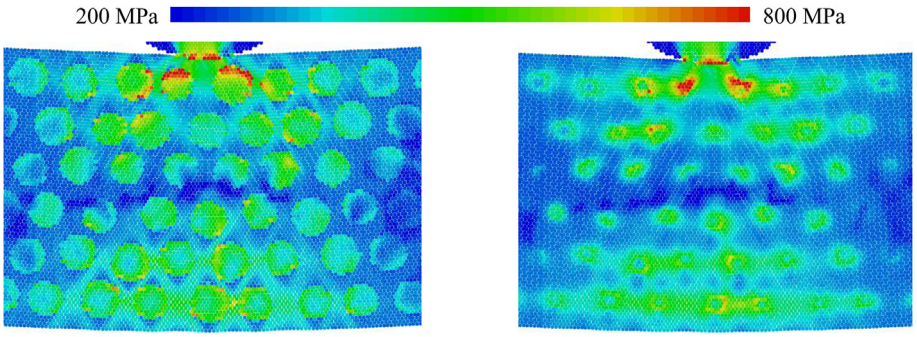

Fig. 12. Von Mises stress distributions in the central part of the model metal–ceramic composite samples with "narrow" (0.1 microns) and "wide" (1 micron) interphase boundaries (the value of bending angle is 3.5°).

in Fig. 14. Thus, the effective elastic modulus and strength of the ceramics obtained from nanocrystalline powders significantly decreased after gel filling (Fig. 14(a)), while the properties of coarse-crystalline ceramics increased (Fig. 14(b)) [47]. Such strange effect may be explained by changing the interface between the matrix and gel inclusions.

To ascertain the nature of changing mechanical properties of ceramics after filling its pores with gel, here we model the uniaxial compression of plane (plain strain) ceramics samples with empty pores as well as with pores filled with gel. It is assumed that fills only the 2 μm and 6 μm sized pores are filled with gel, which have equiaxial shape. The dimensions of sample are 300 × 300 μm. Response function of the automata modeling ceramics [3,4] corresponds to elastic-brittle material (like curve 2 in Fig. 6(b)), response function of the automata modeling gel corresponds to elastic–plastic material with bilinear hardening (like curve 1 in Fig. 6(b)). Large pores of the ceramics are modeled explicitly in the MCA model, while the 1 μm and less sized pores are taken into account implicitly (via the parameters of response function). The fracture criterion of ceramics automata is based on the threshold value of von Mises stress, but for pairs "gel-ceramics" a two-parametric criterion of Drucker–Prager is used.

Total porosity of the modeled samples is 0.30 (this corresponds to 3D porosity about 40%). Each maxima of pore size distribution have fraction of 50%, 25% and 25% of the total porosity.

The size of cellular automata corresponds to the averaged grain size, i.e. is equal to 2 μm. Pore structure is built using two procedures. First procedure assumes only cells of 6 μm sized pores; the second one generates 2 μm sized pores as well as cells of pores. The pores are generated by removing the randomly selected single automata (2 μm sized pores) and their six closed neighbors (cells of pores) from initial closed packing of automata. Thus, in the first procedure, the explicit porosity is of 7.5% and the implicit one is of 22.5%; in the second procedure, the corresponding values are 15% and 15% (Fig. 15).

Analysis of the calculation data shows that the filling pores with gel results in a slight increase in their elastic and strength properties. Young's modulus, Poisson's ratio and strength for the samples in Fig. 15(a) increases by 0.8%, 2.4% and 3.7%, respectively; and for the samples in Fig. 15(b), they increase by 1.5%, 4.3% and 1.3%, respectively. Thus, these changes are smaller for strength and larger for elastic properties.

The fracture patterns of the simulated samples, as networks of inter-automata bonds, are shown in Fig. 16. In all the cases, the samples fails with the system of macrocracks propagating along the lines inclined to the direction of loading. For the samples generated using the first procedure (Fig. 16(a) and

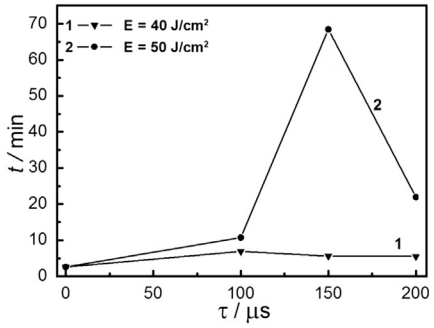

(a) Temporal durability of MCC bars at cutting versus pulse duration for various values of the energy density of electron beam

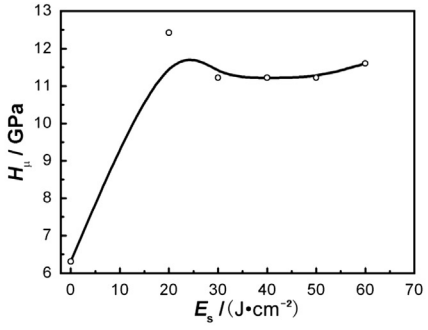

(b) Micro-hardness of MCC surface layer versus energy density of electron beam

Fig. 13. Increase in strength of MMC after electron-beam irradiation in nitrogen-containing gas-discharge plasma.

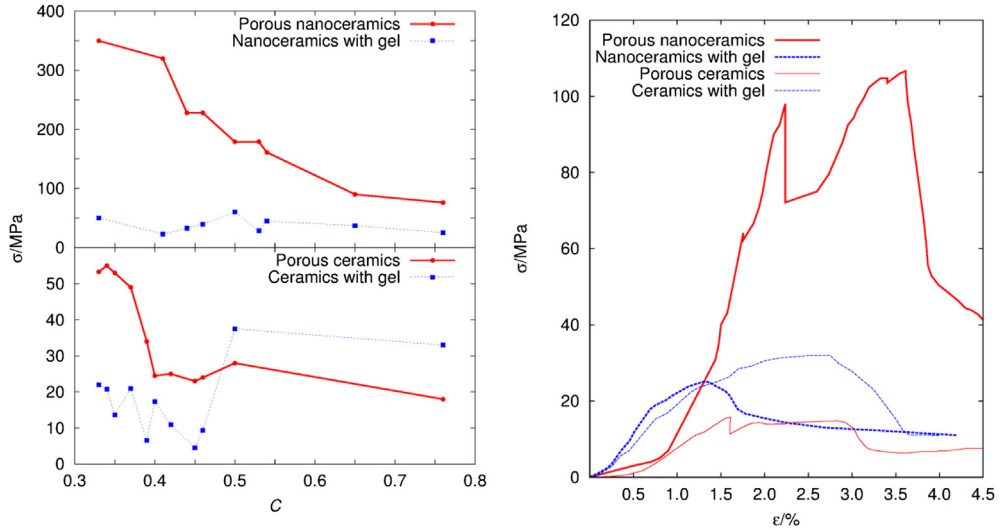

(a) Strength versus porosity of different $ZrO_2(Y_2O_3)$ ceramics samples

(b) Loading diagrams of different $ZrO_2(Y_2O_3)$ ceramics with porosity of 0.8

Fig. 14. Experimental data on the impact of gel filling on mechanical properties of ceramics.

(b)), the cracks are linear and well expressed when the value of explicit porosity is minimal (7.5%). This is because the structure is closed to homogeneous body. For the samples with explicit porosity equaling to 15% (Fig. 16(c) and (d)), the cracks form a "blurred" picture and their path is curved and complicated which can be explained by large number of stress concentrators in the sample.

In all the considered cases, the filling of porous samples with gel leads to the change of distribution of stress concentrators in the samples, in particular makes this distribution more homogenous. Thus the generation and propagation of cracks in the samples with filled pores differ significantly from those of the same sample with empty pores. At that, the fracture pattern of the sample with filled pores is closer to that of homogeneous material [48,49].

In the modeling mentioned above, it was assumed that the gel was fully filled in a pore and had perfectly contacted with ceramics surface. It was not possible to describe the experimental evidence in the framework of that model [47]. Therefore another model, based on the assumption that the gel changes the local elastic and strength properties of the interface "gel-ceramics", was developed at the next step.

The total porosity of the samples in this model was varied from 0.15 to 0.27. Herewith the porosity C_1 corresponding to 1 μm and less sized small pores was equal to 0.1 for all the samples and taken into account implicitly. The size of large pores was equal to 2 μm or 6 μm; the pores were taken into account explicitly, the corresponding porosity C_2 was varied from 0.05 to 0.17. Sample dimension was 300 × 300 μm, and automaton size was 2 μm. Threshold value of von Mises stress was used as a fracture criterion.

Three groups of samples with total porosity of 0.15, 0.21 and 0.27 are considered. The porosities C_2 corresponding to large pores are equal to 0.05; 0.11; and 0.17, thereby forming

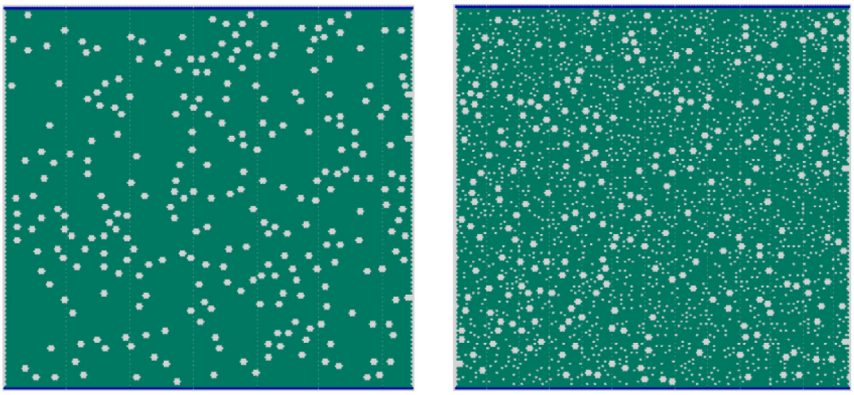

(a) First procedure

(b) Second procedure

Fig. 15. Initial structure of samples obtained with different procedures of pore generation.

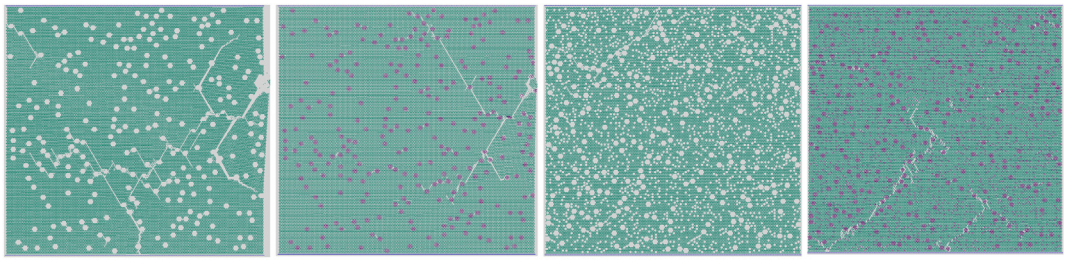

Fig. 16. Networks of inter-automata bonds in the samples generated using different procedures showing fracture patterns in the material.

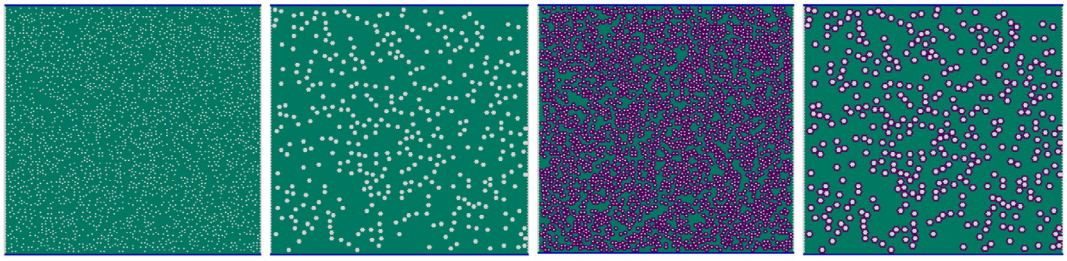

Fig. 17. Initial structures of the modeled samples with different pore size D and properties of the "pore-matrix" interface for explicit porosity $C_2 = 0.11$.

three subgroups. Each subgroup contains six samples with individual spatial distribution of pores.

To model the different effect of a gel on the properties of the interface "gel-ceramics", we vary the elasticity (E_{local}) and strength (σ_{local}) parameters of the response function of the corresponding automata. For pure ceramics, these parameters are $E_0 = 98$ GPa and $\sigma_0 = 730$ MPa. Due to gel effect, the elastic properties was assumed to be improved twice: $E_{\text{local}} = 0.5E_0 = 49$ GPa or $E_{\text{local}} = 2E_0 = 196$ GPa; the strength property $\sigma_{\text{local}} = 0.6\sigma_0 = 438$ MPa or $\sigma_{\text{local}} = 1.4\sigma_0 = 1022$ MPa (i.e. to be improved by ±40%). Typical sample structures for this model are shown in Fig. 17.

Analysis of the calculated results shows that the change of local elastic properties for the "pore-matrix" interface has the most impact on the effective elastic modulus. Fig. 18 shows the effective elastic modulus E_{eff} of the ceramics samples with modified elastic property of "pore-matrix" interface, which is normalized to the modulus $E_{\text{eff\_0}}$ of the corresponding pure ceramics samples versus fraction of pores with modified properties. One can see that changing E_{local} twice leads to change E_{eff} by +10%/−7% for $C_2 = 0.05$, and by +35%/−25% for $C_2 = 0.17$ for the samples with pore size $D = 6$ μm. For the samples with smaller pore size ($D = 2$ μm), this effect is stronger (due to larger value of specific surface of pores): +25%/−23% for $C_2 = 0.05$ and +85%/−48% for $C_2 = 0.17$.

The local strength properties of the interface automata are changed to cause a variation of the effective strength of the composite and its fracture pattern; it does not influence on the effective elastic modulus. Fig. 19 shows the effective strength limit σ_{eff} of the ceramics samples with modified strength property σ_{local} of "pore-matrix" interface, which is normalized to the strength limit $\sigma_{\text{eff\_0}}$ of the corresponding pure ceramics samples versus fraction of pores with modified properties. Thus, changing σ_{local} by ±40% leads to change σ_{eff} by +14%/−22% for $C_2 = 0.05$, and by +19%/−37% for $C_2 = 0.17$ for the samples with pore size $D = 6$ μm (Fig. 19). For the samples with smaller pore size ($D = 2$ μm), this effect is stronger: +27%/−32% for $C_2 = 0.05$ and +40%/−41% for $C_2 = 0.17$.

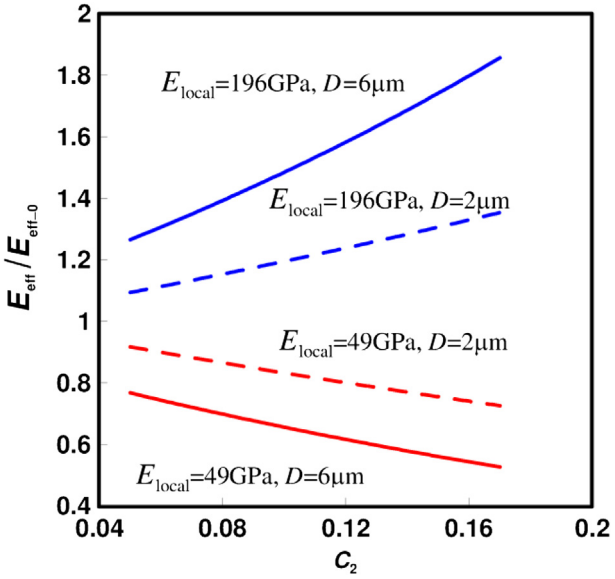

Fig. 18. Normalized effective elastic modulus of ceramics samples with modified elastic property E_{local} of "pore-matrix" interface for different pore size D versus fraction of pores with modified properties.

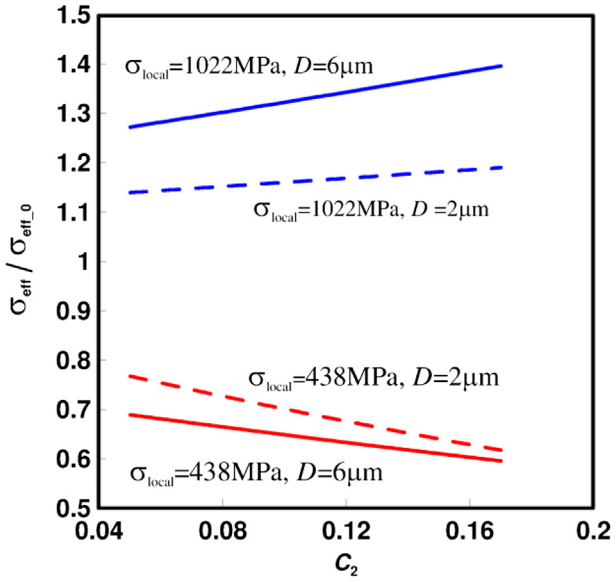

Fig. 19. Normalized effective strength limit of ceramics samples with modified strength property σ_{local} of "pore-matrix" interface for different pore size D versus fraction of pores with modified properties.

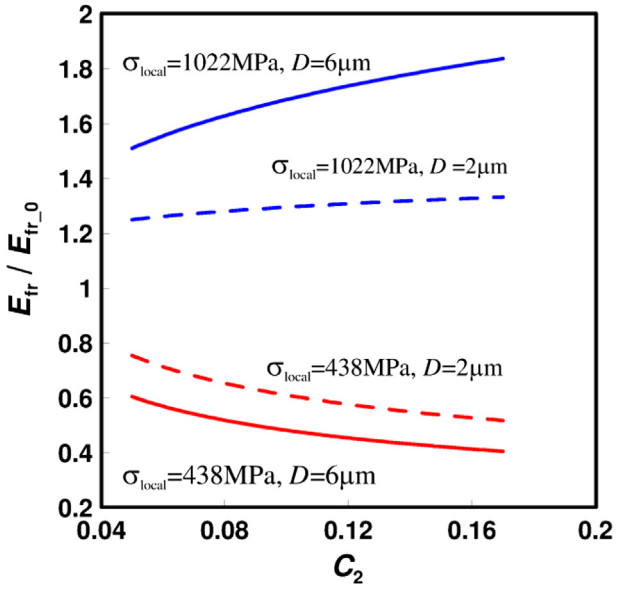

Fig. 21. Normalized specific fracture energy of ceramics samples with modified strength property σ_{local} of "pore-matrix" interface for different pore size D versus fraction of pores with modified properties.

Analysis of specific fracture energy of the model samples (E_{fr}) shows that the increase in local strength property σ_{local} leads to the corresponding increase in E_{fr}, whereas the increasing/decreasing of local elastic property E_{local} leads to decreasing/increasing of E_{fr} (Figs. 20 and 21). As described in the foregoing, this change is stronger for smaller pore size. Thus, the possible influence of gel soaking of ceramics on its dissipative properties is ambiguous, because the fracture energy is defined by both elastic and strength properties of the material. In particular, if the soaking causes the increase in local elastic properties of pore surface, it may result in decreasing the fracture energy, but the increase in the strength properties always results in increasing the fracture energy.

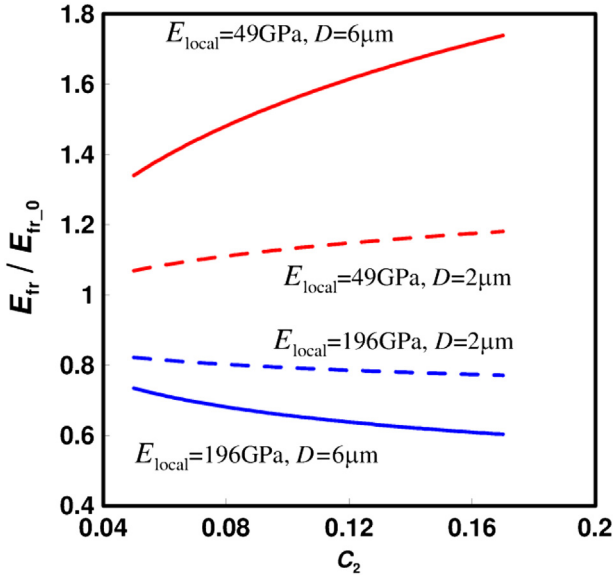

Fig. 20. Normalized specific fracture energy of ceramics samples with modified elastic property E_{local} of "pore-matrix" interface for different pore size D versus fraction of pores with modified properties.

5. Conclusions

Based on movable cellular automaton method, the models for computer-aided studying mechanical behavior of composites with special properties of inclusions and inclusion-matrix interphase were developed.

The influences of strength of reinforcing ceramic particles as well as the mechanical and geometric properties of interphase boundaries on the peculiarities of mechanical response of TiC- reinforced Ni–Cr metal–ceramic composite under dynamic loading were studied using the proposed model. It was shown that the strength of reinforcing particles and the width of particle-binder interphase boundaries had a determining influence on the service characteristics of the metal–ceramic composite. In particular, the increase in strength of carbide inclusions may lead to a significant increase in strength and value of ultimate strain of the composite material. And use of the technologies forming thick interphase boundaries among the carbide inclusions and the matrix during production and processing of the composites allow to enhance their service characteristics.

Based on the example of porous zirconia ceramics, changing the elastic properties of the pore surface mainly leads to the corresponding change in effective elastic modulus of the ceramic samples. But changing the strength properties of the pore surface leads to the change in effective strength limit of the samples only. The less the pore size is, the more this effect is. It is interesting that the fracture energy of the ceramics with increased elastic properties of the pore surface may reduce. This effect may explain the peculiarities of mechanical behavior of gel-filled zirconia ceramics.

Acknowledgments

The investigation has been carried out at partial financial support of the Projects Nos. III.23.2.3 (I.S. Konovalenko, S.P. Buyakova) and III.23.2.4 (S.G. Psakhie) of the Basic Scientific Research Program of State Academies of Sciences for 2013−2020, the RFBR Project No. 12-01-00805-a (A.Yu. Smolin, E.V. Shilko), and the grant No. 14-19-00718 of the Russian Science Foundation (A.Yu. Smolin, E.V. Shilko, S.V. Astafurov).

References

[1] Yu B, Ovcharenko VE, Psakhie SG, Lapshin OV. Electron-beam treatment of tungsten-free TiC/NiCr cermet II: structural transformations in the subsurface layer. J Mater Sci Technol 2006;22(4):511−3.
[2] Chawla N, Chawla KK. Metal matrix composites. New York: Springer; 2006.
[3] Kulkov SN. Structure, phase composition and mechanical properties of ZrO_2-based nanosystems. Phys Mesomech 2008;11(1−2):29−41.
[4] Buyakova SP, Wei H, Dunmy L, Haiyun C, Sablina TYu, Mel'nikov AG, Kul'kov SN. Mechanical behavior of porous zirconium dioxide under active deformation by compression. Tech Phys Lett 1999;25(9):695−6.
[5] Shen J, Ren X. Experimental investigation on transmission of stress waves in sandwich samples made of foam concrete. Def Technol 2013;9(2):110−4.
[6] Konovalenko IgS, Smolin AYu, Korostelev SYu, Psakhe SG. Dependence of the macroscopic elastic properties of porous media on the parameters of a stochastic spatial pore distribution. Tech Phys 2009;54(5):758−61.
[7] Psakhie S, Ovcharenko V, Yu B, Shilko E, Astafurov S, Ivanov Yu, Byeli A, Mokhovikov A. Influence of features of interphase boundaries on mechanical properties and fracture pattern in metal−ceramic composites. J Mater Sci Technol 2013;29(11):1025−34.
[8] Dimaki AV, Shil'ko EV, Psakh'e SG. Simulating the propagation of exothermic reactions in heterogeneous media. Combust Explos Shock Waves 2005;41(2):151−7.
[9] Oñate E, Rojek J. Combination of discrete element and finite element methods for dynamic analysis of geomechanics problems. Comput Method Appl Mech Eng 2004;193:3087−128.
[10] Johnson GR, Stryk RA. Conversion of 3D distorted elements into meshless particles during dynamic deformation. Int J Impact Eng 2003;28:947−66.
[11] Munjiza AA, Knight EE, Rougier E. Computational mechanics of discontinua. Chichester: Wiley; 2012.
[12] Cundall PA. A discontinuous future for numerical modeling in geomechanics. Geotechn Eng 2001;149(1):41−7.
[13] Psakhie SG, Smolin AYu, Tatarintsev EM. Discrete approach to study fracture energy absorption under dynamic loading. Comput Mater Sci 2000;19:179−82.
[14] Österle W, Dmitriev AI. Functionality of conventional brake friction materials − perceptions from findings observed at different length scales. Wear 2011;271(9−10):2198−207.
[15] Morris JP, Rubin MB, Blair SC, Glenn SA, Heuze FE. Simulations of underground structures subjected to dynamic loading using the distinct element method. Eng Comput 2004;21:384−408.
[16] Dimaki AV, Popov VL. The method of reduction of dimensionality and its application to simulation of elastomer friction under complex dynamic loads. Phys Mesomech 2012;15(5−6):319−23.
[17] Kuznetsov VP, Smolin IYu, Dmitriev AI, Konovalov DA, Makarov AV, Kiryakov AE, Yurovskikh AS. Finite element simulation of nanostructuring burnishing. Phys Mesomech 2013;16(1):62−72.
[18] Griffiths DV, Mustoe GGW. Modelling of elastic continua using a grillage of structural elements based on discrete element concepts. Int J Numer Methods Eng 2001;50:1759−75.
[19] Wang G, Al-Ostaz A, Cheng AH-D, Mantena PR. Hybrid lattice particle modeling: theoretical considerations for a 2D elastic spring network for dynamic fracture simulations. Comput Mater Sci 2009;44:112634.
[20] Psakhie SG, Ostermeyer GP, Dmitriev AI, Shilko EV, Smolin AYu, Korostelev SYu. Method of movable cellular automata as a new trend of discrete computational mechanics. I. Theoretical description. Phys Mesomech 2000;3(2):5−12.
[21] Psakhie SG, Horie Y, Ostermeyer G-P, Korostelev SYu, Smolin AYu, Shilko EV, et al. Movable cellular automata method for simulating materials with mesostructure. Theor Appl Fract Mech 2001;37(1−3):311−34.
[22] Popov VL, Psakhie SG. Theoretical principles of modeling elastoplastic media by movable cellular automata method. I. Homogeneous media. Phys Mesomech 2001;4(1):15−25.
[23] Mikhailov AS. Foundations of synergetics I. Distributed active systems. Berlin: Springer; 1994.
[24] Wiener N, Rosenblueth A. The mathematical formulation of the problem of conduction of impulses in a network of connected excitable elements, specially in cardiac muscle. Arch Inst Cardiol Mex 1946;16(3−4):205−65.
[25] Psakhie SG, Horie Y, Korostelev SYu, Smolin AYu, Dmitriev AI, Shilko EV, et al. Method of movable cellular automata as a tool for simulation within the framework of mesomechanics. Russ Phys J 1995;38(11):1157−68.
[26] Smolin AYu, Roman NV, Dobrynin SA, Psakhie SG. On rotation in the movable cellular automaton method. Phys Mesomech 2009;12(3−4):124−9.
[27] Psakhie S, Shilko E, Smolin A, Astafurov S, Ovcharenko V. Development of a formalism of movable cellular automaton method for numerical modeling of fracture of heterogeneous elastic−plastic materials. Fratt Int Strutt 2013;24:26−59.
[28] Cundall PA, Strack ODL. A discrete numerical model for granular assemblies. Geotechnique 1979;29(1):47−65.
[29] Jing L, Stephansson O. Fundamentals of discrete element method for rock engineering: theory and applications. Oxford: Elsevier; 2007.
[30] Sibille L, Nicot F, Donze FV, Darve F. Material instability in granular assemblies from fundamentally different models. Int J Numer Anal Methods Geomech 2007;31(3):457−81.
[31] Martin CL, Bouvard D. Study of the cold compaction of composite powders by the discrete element method. Acta Mater 2003;51(2):373−86.
[32] Potyondy DO, Cundall PA. A bonded-particle model for rock. Int J Rock Mech Min Sci 2004;41(8):1329−64.
[33] Psakhie SG, Shilko EV, Smolin AYu, Dimaki AV, Dmitriev AI, Konovalenko IgS, Astafurov SV, Zavshek S. Approach to simulation of deformation and fracture of hierarchically organized heterogeneous media, including contrast media. Phys Mesomech 2011;14(5−6):224−48.
[34] Wilkins ML. Computer simulation of dynamic phenomena. Berlin: Springer-Verlag; 1999.
[35] Smolin AYu, Roman NV, Konovalenko IgS, Eremina GM, Buyakova SP, Psakhie SG. 3D simulation of dependence of mechanical properties of porous ceramics on porosity. Eng Fract Mech 2014;130:96−115.
[36] Kainer KU. In: Kainer KU, editor. Metal matrix composites: custom-made materials for automotive and aerospace engineering. Weinheim: Wiley-VCH Verlag; 2006.
[37] Pramanik A, Zhang LC, Arsecularatne JA. Prediction of cutting forces in machining of metal matrix composites. Int J Mach Tool Manuf;46(14):1795−1803.
[38] Vityaz PA, Grechikhin LI. Nanotechnology for producing titanium-based cermets. Phys Mesomech 2004;7(5−6):51−6.
[39] Ayyar A, Chawla N. Microstructure-based modeling of crack growth in particle reinforced composites. Compos Sci Technol 2006;66:1980−94.
[40] Mortensen A, Llorca J. Metal matrix composites. Annu Rev Mater Res 2010;40:243−70.
[41] Psakhie SG, Horie Y, Shilko EV, Smolin AYu, Dmitriev AI, Astafurov SV. Discrete element approach to modeling heterogeneous

elastic−plastic materials and media. Int J Terrasp Sci Eng 2011;1:93−125.
[42] Xing MZ, Wang YG, Jiang ZX. Dynamic fracture behaviors of selected aluminum alloys under three-point bending. Def Technol 2013;9(4):193−200.
[43] Sket F, Seltzer R, Molina-Aldareguía JM, González C, Llorca J. Determination of damage micromechanisms and fracture resistance of glass fiber/epoxy cross-ply laminate by means of X-ray computed microtomography. Compos Sci Technol 2012;72:350−9.
[44] Ovcharenko VE, Yu B, Psakhie SG. Electron-beam treatment of tungsten-free TiC/NiCr cermet. I: influence of subsurface layer microstructure on resistance to wear during cutting of metals. J Mater Sci Technol 2005;21(3):427−9.
[45] Ovcharenko VE, Mokhovikov AA, Ignat'ev AS. Influence of surface nanostructure on the life of cermet in metal cutting. Steel Transl 2013;43(6):348−50.
[46] Altunina LK, Kuvshinov VA, Stasieva LA. Thermoreversible polymer gels for enhanced oil recovery. Chem Sustainable Dev 2011;19:121−30.
[47] Development of scientific principles for the construction of a new class of contrast materials with nanocomposite gels as a functional filler. Tomsk: Institute of Petroleum Chemistry SB RAS; 2013. Report on interdisciplinary integration project No 66 of the Siberian Branch of the Russian Academy of Sciences, [in Russian].
[48] Skripnyak VA, Skripnyak EG, Kozulin AA, Skripnyak VV, Korobenkov MV. Computer simulation of the relation between mechanical behavior and structural evolution of oxide ceramics under dynamic loading. Russ Phys J 2009;52(12):1300−8.
[49] Kostandov YuA, Makarov PV, Eremin MO, Smolin IYu, Shipovskii IE. Fracture of compressed brittle bodies with a crack. Int J Appl Mech 2013;49(1):95−101.